2023

Achieving Strong Chemical Interface and Superior Energy-Saving Capability at the Crosslinks of Rubber Composites Containing Graphene Oxide Using Thiol-Vinyl Click Chemistry

Rui Zhang
University of Chemical Technology, China

Jiaye Li
Beijing University of Chemical Technology, Beijing, China

Zongchao Xu
Beijing University of Chemical Technical, China

See next page for additional authors

Funder: This work was supported by the National Key R&D Program of China (2017YFE0126800) and the National Natural Science Foundation of China (51790504).

Achieving strong chemical interface and superior energy-saving capability at the crosslinks of rubber composites containing graphene oxide using thiol-vinyl click chemistry

Rui Zhang [a, b], Jiaye Li [a, b], Zongchao Xu [a, b], Stephen Jerrams [c], Shui Hu [a, b], Li Liu* [a, b], Shipeng Wen* [a, b], Liqun Zhang [a, b]

a State Key Laboratory of Organic-Inorganic Composites, Beijing University of Chemical Technology, Beijing 100029, China

b Beijing Engineering Research Center of Advanced Elastomers, Beijing University of Chemical Technology, Beijing 100029, China

c Technological University Dublin, Dublin 00000, Ireland

*Corresponding Author

E-mail: wensp@mail.buct.edu.cn (Prof. Dr. Shipeng Wen), liul@mail.buct.edu.cn (Prof. Dr. Li Liu)

Abstract

Rapidly developments in international transportation inevitably lead to an increase in the consumption of energy and resources. Minimizing the rolling resistance of tires in this scenario is a pressing challenge. To lower the rolling resistance of tires, enhancing the interaction between fillers and rubber molecules while improving the dispersion of fillers are required to reduce the internal mutual friction and viscous loss of rubber composites. In this study, graphene oxide (GO) was modified using γ-mercaptopropyltrimethoxysilane (MPTMS) with thiol groups. A modified GO/natural rubber (MGO/NR) masterbatch with a fine dispersion of MGO was then introduced into solution-polymerized styrene butadiene rubber (SSBR) to create an MGO/SiO_2/SSBR composite. During the crosslinking process at high temperatures, a strong chemical interface interaction between the MGO and rubber molecules was formed by the thiol-vinyl click reaction. The MGO sheets also act as crosslinks to enhance the crosslinking network. The results showed that the rolling resistance of the MGO SiO_2/SSBR composite was superior by 19.4% and the energy loss was reduced by 15.7% compared with that of the base SiO_2/SSBR composite. Strikingly, the wear performance and wet skid resistance improved by 19% and 17.3%, respectively. These results showed a strong interface that not only improved rolling resistance performance but also contributed to balancing the "magic triangle" (the combination of wear resistance, fuel efficiency, and traction) properties of tires.

Keywords: rubber, graphene oxide, interface, energy-saving, rolling resistance

1. Introduction

At present, the consumption of nonrenewable energy is a worldwide problem that requires heightened attention in the international transportation industry. This is because worldwide transportation energy consumption accounts for more than 20% of the total energy dissipated, whereas the energy consumed by automobiles accounts for approximately 6.6% of the total energy [1]. It has been reported [2-4] that rolling resistance of the tires accounts for 40% of the fuel consumption of an automobile. It is estimated that every 10% reduction in tire rolling resistance will reduce fuel consumption by approximately 2% [5]. Consequently, it is of paramount importance to save non-renewable energy by reducing the rolling resistance of the tires.

According to the "Tire Labelling Regulation (EC NO. 1222/2009)" [6], the rolling resistance of tires is heavily associated with the energy dissipation induced by the cyclic deformation of the tire during driving [1, 7]. The energy dissipated during tire deformation is primarily generated by the dynamic hysteresis loss of rubber composites, which mainly includes the mutual friction between rubber molecule chains, between rubber molecule chains and nanoparticles, and between nanoparticles and nanoparticles [8, 9].

In general, the improvement in tire rolling resistance has been considered from the following three perspectives: (1) the mutual friction between the fillers can be reduced by improving their dispersion; (2) the mutual friction between fillers and rubber molecules can be reduced by enhancing the interfacial interaction between them; and (3) the entanglements and mutual friction between molecules can be decreased by moderately increasing the crosslinking degree of rubber molecules.

Currently, silica nanoparticles are mainly used to reinforce rubber composites for green tires owing to their excellent performance in improving wet skid resistance and reducing rolling resistance [9-12]. Therefore, research on the dispersion and interfacial interactions of silica in rubber matrices has attracted significant attention. Zhai et al. [4] reported the successful synthesis of a series of novel silane coupling agents by transesterification of the fatty alcohol polyoxyethylene ether-9 (AEO-9) with Si69. Novel silane coupling agents were used to enhance the interfacial interaction of silica in the

rubber matrix. As a result, the rolling resistance of the rubber composites was reduced by 12.1% compared to that of traditional samples. Tang et al. [7] utilized a phosphonium ionic liquid (PIL) as a novel catalyst to increase the silanization of silica with bis(3-triethoxysilylpropyl)-tetrasulfide (TESPT). The interfacial adhesion of silica and rubber molecules was greatly enhanced, resulting in a 36.78% reduction in energy loss during vehicle operation.

Graphene oxide (GO) with a high specific surface area and abundant reactive functional groups has been introduced into rubber composites [13-16]. It was found that the addition of lamellar GO was beneficial to enhance the dispersion of spherical fillers in a rubber matrix, leading to a reduction in the mutual friction between fillers and an improvement in the rolling resistance of rubber composites. For example, Yang et al. [17] studied the effects of substituting GO for carbon black (CB) on the structure and performance of CB/NR composites. The results showed that the addition of a small amount of GO was beneficial to improving the CB dispersion and decreasing filler friction during dynamic loading in service. Zhang et al. [18] investigated the influence of the partial substitution of CB with GO on the crosslink structure and properties of NR composites. The results showed that the dispersion of CB was improved by introducing a few GO nanosheets, thereby improving the dynamic and static mechanical properties. However, it is noted that most rubber composites filled with silica or GO were prepared by melt compounding [19]. As a consequence, it was difficult to further improve the filler dispersion in the rubber matrix, leading to problems when attempting to modify the rolling resistance of silica/rubber composites. In addition to the interfacial interaction between the filler and the rubber molecules, it is also important to reduce the mutual friction between them. Therefore, it remains a challenge to improve the rolling resistance of rubber composites by simultaneously achieving a fine filler dispersion and a strong filler/rubber interface.

In this study, GO was functionalized with γ-mercaptopropyltrimethoxysilane (MPTMS) containing thiol groups. The modified GO (MGO) was compounded with natural rubber (NR) via latex compounding and subsequent coagulation. The MGO/NR masterbatch with finely dispersed MGO was further introduced into solution-polymerized

styrene butadiene rubber (SSBR) to obtain an MGO/SiO_2/SSBR composite. During the crosslinking process at high temperature, strong chemical interface interactions between MGO and SSBR molecules were developed by the thiol-vinyl click reaction, resulting in MGO sheets constituting part of the network crosslinking points. This novel dispersion and interfacial structure led to the wear performance and wet skid resistance of the MGO/SiO_2/SSBR composite being improved by 19% and 17.3%, respectively, and the rolling resistance and energy loss of the MGO/SiO_2/SSBR decreased by 19.4% and 15.7%, respectively, compared with those of the SiO_2/SSBR composite.

2. Experimental section

2.1 Materials

GO was synthesized using a modified Hummers method. NR latex (solid content: 60%) was purchased from Thr Latex Co., Ltd. Solution polymerized styrene-butadiene rubber (SSBR, Kumho 6270) was purchased from Kumho Petrochemical Co., LTD. γ-mercaptopropyltrimethoxysilane (MPTMS) was provided by Beijing Mairuida Technology Co., LTD (China). Zinc oxide (ZnO), stearic acid (SA), N-1,3-dimethylbutyl-N'-phenyl-p-phenylenediamine (6ppd), silica (SiO_2, VN3), N-Cyclohexyl-2-benzothiazolesulfenamide (CZ), and sulfur were all commercially available and used without any treatment.

2.2 Samples preparation

2.2.1 Preparation of MGO

A 2 mg/mL GO suspension was prepared by sonication for 30 min. MPTMS deionized water/ethanol (1/8, v/v) was sonicated for 1 h until it was completely hydrolyzed. Then, the hydrolysate of MPTMS in deionized water/ethanol was added to the GO suspension. The reaction was carried out at 68 °C for 6 h. Then, the mixture was washed several times using a centrifuge to remove the unreacted MPTMS. After Soxhlet extraction, the modified GO was again mixed with deionized water to form a 2 mg/mL suspension, which was labeled as MGO.

2.2.2 Preparation of MGO/SiO_2/SSBR composites

GO was easily aggregated owing to the strong hydrogen bonding and van der Waals

forces, resulting in the deterioration of the dynamic and static mechanical properties of the rubber nanocomposites. Thereafter, the GO/natural rubber (NR) masterbatch was prepared as described in our previous report [20]. To characterize the dispersion of GO in NR, the GO/NR masterbatch was further compounded with SSBR to obtain SiO_2/SSBR, GO/SiO_2/SSBR, and MGO/SiO_2/SSBR compounds.

Table 1 shows the main composition of SSBR composites. The parts by weight per hundred-part rubber (phr) of rubber integrates are listed in Table 1. These raw materials were mixed on a two-roll mill to obtain the compounds. Then, the compounds were cured at 150 °C under a pressure of 15 MPa to obtain SiO_2/SSBR, GO/SiO_2/SSBR and MGO/SiO_2/SSBR composites.

Table 1. The formula of the rubber composites

Materials (phr)	SiO_2/SSBR	GO/SiO_2/SSBR	MGO/SiO_2/SSBR
SSBR	85	85	85
NR	15	15	15
SiO_2	65	65	65
GO	0	2	0
MGO	0	0	2
ZnO	3	3	3
SA	2	2	2
RD	2	2	2
6ppd	2	2	2
NS	2	2	2
sulfur	1.8	1.8	1.8

2.3 Characterization

The dispersion of the filler in the rubber composites was observed using a G220 S-TWIN transmission electron microscope (TEM; FEI Co., USA). The surface regularity of GO and MGO was characterized via Raman spectroscopy (Renishaw Co., England). The laser wavelength was 514 nm, and the laser intensity was 10%. The spectra were recorded within wavenumbers ranging from 240 to 2500 cm^{-1}. Elemental analysis of GO and MGO was performed using an ESCALAB 250 X-ray photoelectron spectrometer (XPS; Thereto Electron Co., USA). C, O, N, and Si were scanned using an Al-Kα X-ray source (1486.6

eV). The exfoliated structures of GO and MGO were characterized using D/Max2500 X-ray diffraction analysis (XRD, Rigaku Co., Japan). The scan range was 5–90°, and the scan rate was 5° min^{-1}. The chemical structures of GO and MGO were recorded using a Tensor 27 Fourier-transform infrared (FTIR) spectrometer (Bruker Optik Gmbh Co., Germany). The spectra were recorded within wavenumbers ranging from 400 to 4000 cm^{-1}. The weight losses of GO and MGO were identified using a TGA-1 thermogravimetric analyzer (Mettler-Toledo Co., Switzerland). Thermogravimetric Analysis (TGA) was performed at a heating rate of 10 °C /min under a nitrogen atmosphere. The filler network and dynamic performance of the rubber composites were characterized using an RPA 2000 (Alpha Technologies Co., USA). For rubber compounds, the strain range was 0.1–200%, the test frequency was set to 1 Hz, and the test temperature was set to 60 °C. For the cured rubber composites, the strain range was 0.1–42%, the test frequency was set to 10 Hz, and the test temperature was set to 60 °C. The dynamic mechanical properties of all rubber composites were investigated using a VA3000 dynamic mechanical thermal analyzer (DMTA, METRAVIB Corporation, France). The test was performed in tensile mode at 10 Hz. The temperature ranged from -65 to 65 °C at a heating rate of 3 °C /min. Three samples of each composite were prepared for the DMTA testing. The static mechanical performance of the rubber composites was characterized using a CTM4104 electrical tensile tester (Shenzhen SANS Test Machine Co., China), according to the ISO 37:2005 standard. The abrasion performance of all the rubber composites was tested using a GT-7012-D DIN abrasion machine (Mingzhu Machinery Co., Ltd., China) in accordance with ISO 4649. The crosslinking densities of the rubber composites were measured by nuclear magnetic resonance (NMR) spectroscopy (VTMR20-010V-1, Suzhou Niumag Corporation, China). A rubber wheel rolling resistance test was performed using an RSS-II model rolling resistance testing machine (Beijing WANHUI Technology Co., Ltd., China). The load and rotation speed were 30 kg and 600 rpm (revolutions per minute), respectively.

3. Results and discussion

3.1 Design and preparation of MGO/SiO_2/SSBR composites

The design and preparation of the MGO/SiO_2/SSBR composites are illustrated in Figure 1. The thiol groups were grafted onto the surface of GO in the aqueous phase by MPTMS modification, resulting in exfoliation of the GO sheets. Thereafter, an MGO/NR masterbatch was prepared to enhance the dispersion of MGO in the rubber composites. Furthermore, the thiol groups of MGO reacted with the vinyl groups of the rubber molecules by thermal treatment during the crosslinking reaction, thereby strengthening the interfacial interaction between the MGO and SSBR molecule chains (see the "Experimental Section" for a detailed process).

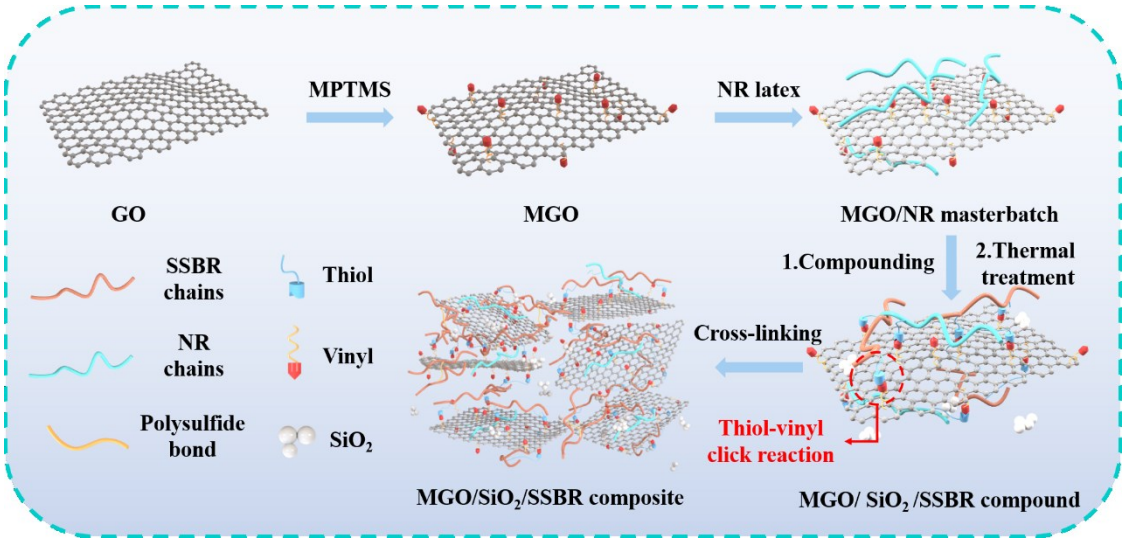

Figure 1. Schematic of the preparation process of MGO/SiO_2/SSBR composites

3.2 Characterizations of GO and MGO

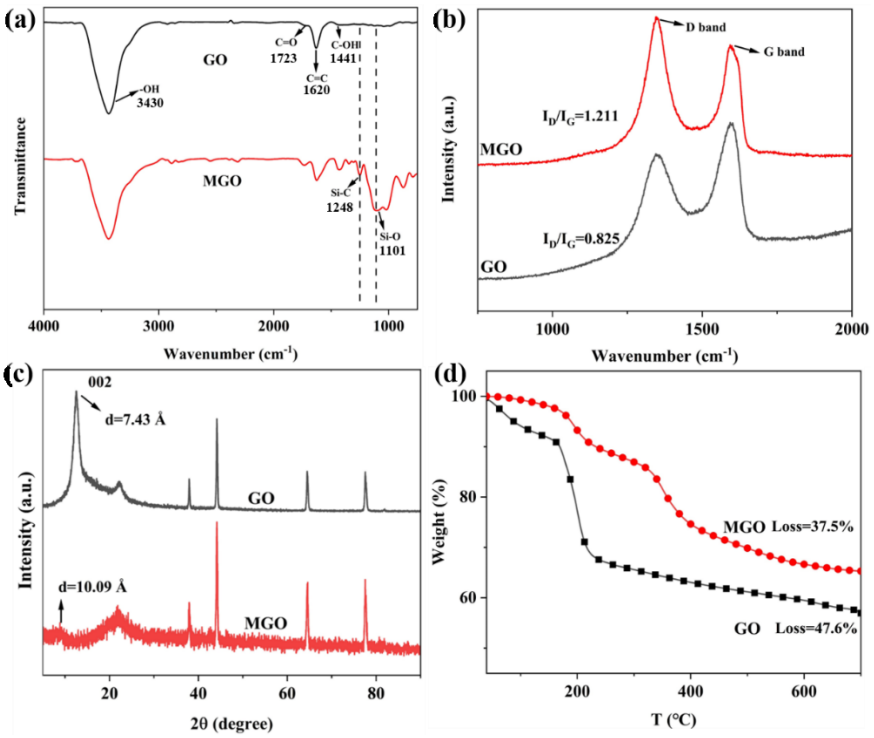

Figure 2. (a) FTTIR spectra, (b) Raman spectra, (c) XRD patterns, and (d) TGA curves of GO and MGO

The FTIR spectra in Figure 2a were used to verify the modification of GO with MPTMS. In the spectrum of GO, the peaks at 3430 and 1723 cm^{-1} are attributed to -OH and C=O stretching vibrations, respectively [21]. The peaks at 1620 and 1441 cm^{-1} are attributed to the C=C stretching vibrations of the aromatic ring skeleton and C-OH deformation vibrations, respectively [22]. These peaks were characteristic of GO. The characteristic peaks of GO appeared in the spectrum of MGO. The Si-C and Si-O stretching vibrations of MPTMS also appeared at 1248 cm^{-1} and 1101 cm^{-1}, respectively [23], indicating that MPTMS was successfully grafted onto the surface of the GO sheets.

The Raman spectra in Figure 2b show that the D and G bands of GO and MGO are located at 1349 and 1599 cm^{-1}, respectively [24]. The D band indicates a C-atom lattice defect on the GO surface. The higher the intensity of the D band, the greater the occurrence of lattice defects of the C atom on the GO. After GO was modified by MPTMS, the ratio of I_D/I_G increased from 0.825 for GO to 1.211 for MGO. This was attributed to the grafting of MPTMS on the GO surfaces, resulting in an increase in the C atom lattice

defects on the GO.

The XRD patterns in Figure 2c show that the diffraction peak of GO was located at 11.8° [25]. After modification by MPTMS, the diffraction peak of MGO decreased and moved to 9.4°. According to the calculation using the Bragg equation, the interplanar crystal spacings on the 002 crystallographic plane of GO and MGO are 7.43 Å and 10.09 Å, respectively. The enlarged space was caused by the intercalation of MPTMS into the GO sheets, resulting in exfoliation of the GO sheets.

The TGA curves in Figure 2d show the TGA curves of GO and MGO. The weight losses of GO and MGO were 47.6% and 37.5%, respectively, indicating that the thermal stability of GO was improved after modification by MPTMS.

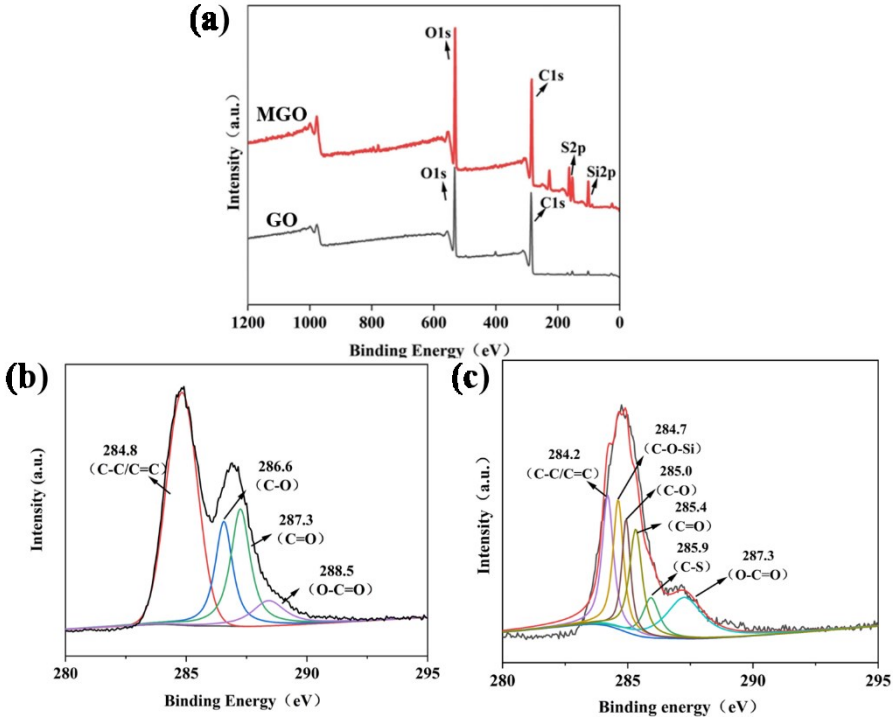

Figure 3. XPS spectra of (a) element survey of GO and MGO, C1s analysis of (b) GO, and (c) MGO

Figure 3 shows the XPS spectra of GO and MGO. Figure 3a shows that the characteristic peaks of S2p and Si2p originate from MPTMS. The C/O ratio decreased from 2.69 (GO) to 2.01 (MGO), indicating that more carboxyl groups were consumed during the esterification reaction. Figures 3b and c showed that the intensities of the C-O, C=O, and O-C=O groups of GO decreased after MPTMS modification. Also, Figure 3c showed the new peaks for C-O-Si and C-S appearing at 284.7 eV and 285.9 eV in the

curves of MGO [26, 27], indicating that the MPTMS was successfully grafted onto the surface of GO.

3.3 The thiol-vinyl click reaction between MGO and SSBR molecules

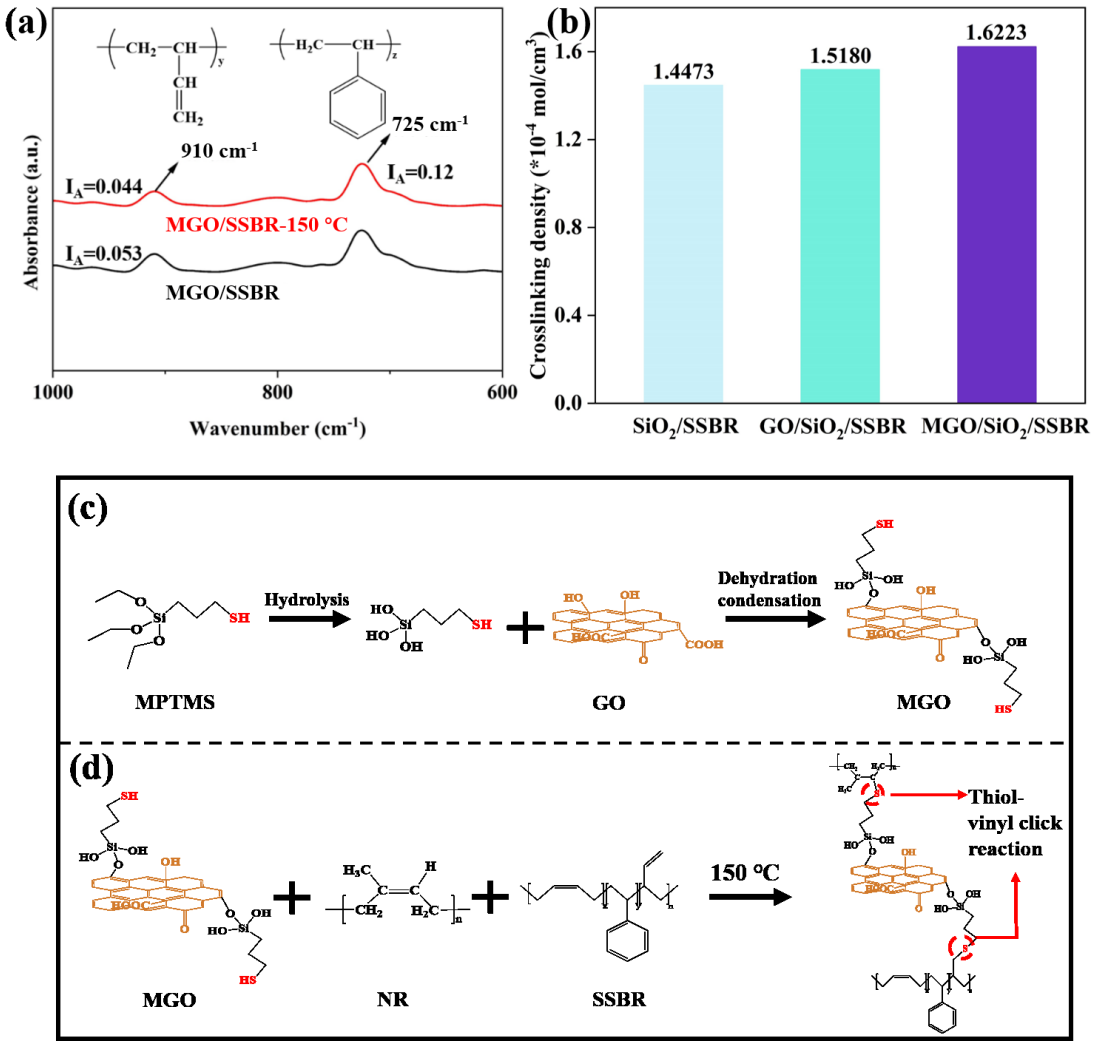

Figure 4. (a) ATR-FTIR spectra of MGO/SSBR composites without sulfur and vulcanizing accelerators. The samples were obtained at room temperature and 150 °C, respectively; (b) the NMR crosslinking densities of SiO_2/SSBR, GO/SiO_2/SSBR and MGO/SiO_2/SSBR composites; the reaction process of (c) dehydration condensation between GO and MPTMS, and (d) the grafting reaction between SSBR and MGO

ATR-FTIR was employed to verify that the thiol groups of MGO reacted with the vinyl groups of rubber molecules. In Figure 4a, the peaks at 725 and 910 cm^{-1} are attributed to the planar vibrations of the styrene rings and vinyl stretching vibrations [28].

After the reaction at a high temperature, the styrene ring content was stable, and the relative absorption intensity of styrene was 0.12. However, the relative absorption intensity of vinyl decreased from 0.053 to 0.044, indicating that some of the vinyl groups of the SSBR reacted with the thiol groups of the MGO. Therefore, a thiol-vinyl click reaction was successfully achieved during the crosslinking reaction at high temperatures. As shown in Figure 4b, the crosslinking density of MGO/SiO_2/SSBR was higher than that of the other two composites, indicating that the MGO sheets acted as crosslinking points and enhanced the crosslinking network. The reaction mechanism between MPTMS and GO is shown in Figure 4 (c, d).

3.4 Dispersion of filler in the SSBR matrix

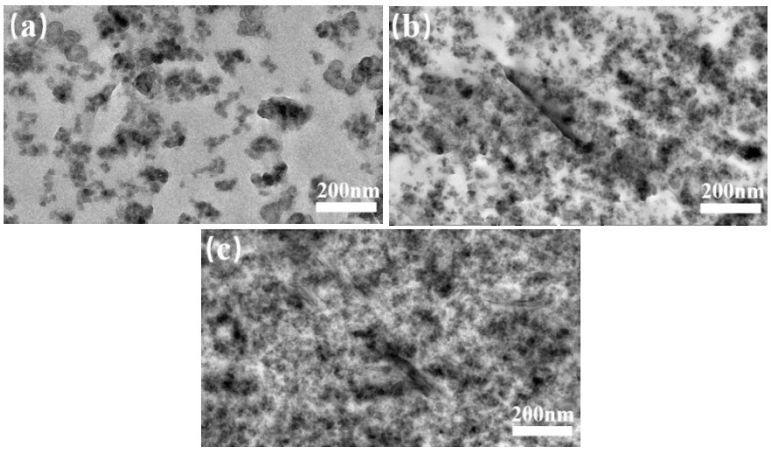

Figure 5. TEM images of (a) SiO_2/SSBR, (b) GO/ SiO_2/SSBR and (c) MGO/SiO_2/SSBR composites

EM was employed to verify the dispersion of nanofillers in the rubber matrix. In Figure 5a, for the SiO_2/SSBR composite, the distribution of SiO_2 is not uniform in the rubber matrix, and there are a large number of agglomerations of SiO_2. As shown in Figure 5b, for the GO/SiO_2/SSBR composite, the GO sheets penetrated the SiO_2 aggregates and improved the dispersion of SiO_2 nanoparticles. However, numerous unaffected areas remained in the matrix. As shown in Figure 5c, for the MGO/SiO_2/SSBR composites, the dispersion of the SiO_2 and GO sheets was improved. This was attributed to the reduction in the oxygen-containing functional groups of GO after MPTMS modification, which prevented aggregation of the GO sheets.

3.5 The dispersion state of MGO and the filler networks in SSBR composites

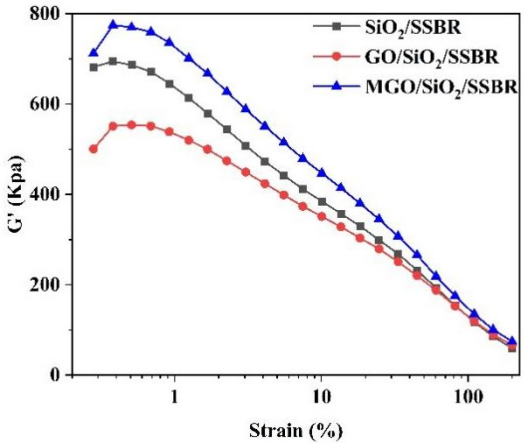

Figure 6. Energy storage moduli-strain curves of SiO_2/SSBR, GO/SiO_2/SSBR and MGO/SiO_2/SSBR compounds

Figure 6 shows the dependence of the storage energy moduli (G') of different SSBR compounds on strain. The G' values of all SSBR compounds initially increased at low strains before declining as the strain increased. The reason for the high values of G' at low strains was the agglomeration of the filler in the compound [29]. As the strain increased, the filler network was gradually destroyed, leading to lower G' values for the compound. Compared with the SiO_2/SSBR compound, the G' value for the GO/SiO_2/SSBR compound was lower, indicating that the GO sheets broke up the agglomerations of SiO_2 and increased the dispersion of SiO_2 in the rubber matrix. Compared with the SiO_2/SSBR compound, the G' value of the MGO/SiO_2/SSBR compound was higher. This was attributed to the MGO sheets acting as crosslinking points, which enhanced the crosslinking of the network. Meanwhile, the enhanced interface between GO and rubber molecules contributed to the higher values of G'.

3.6 Interfacial interaction between MGO and SSBR molecules

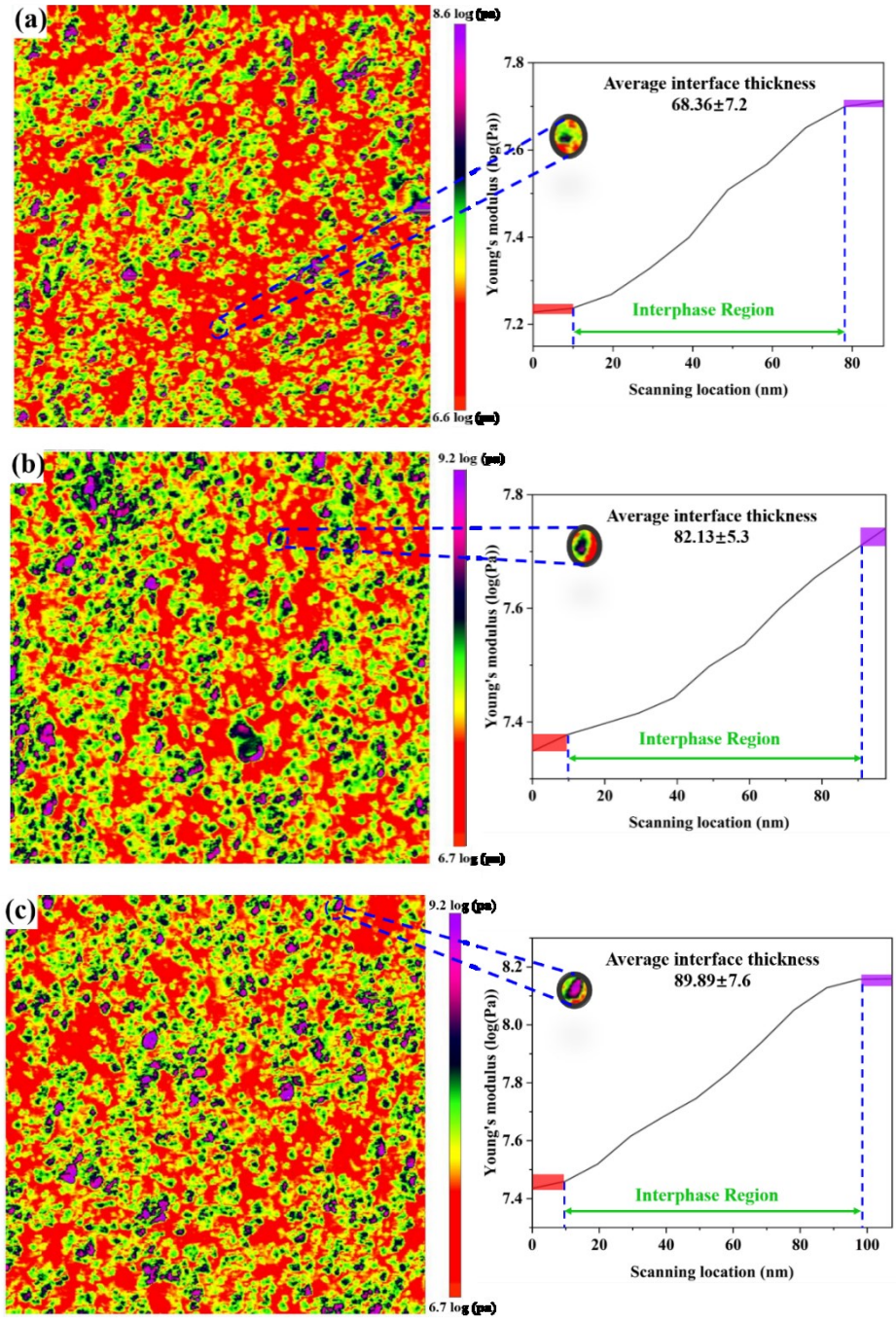

Figure 7. Young's modulus maps of (a) SiO_2/SSBR, (b) GO/SiO_2/SSBR and (c) MGO/SiO_2/SSBR composites and their corresponding modulus profiles across the interface

To further characterize the interface between the fillers and rubber matrices, the peak force-quantitative nanoscale mechanical (PF-QNM) technique was used to measure the gradient change in the Young's modulus of different SSBR composites. The thicknesses

of the interphases between the filler and rubber molecular chains were evaluated quantitatively [30]. Figure 7 shows that the MGO/SiO_2/SSBR composite had the broadest average interface thickness (89.89±7.6 nm) among the three composites. This indicates that MGO exerted a strong restriction on the rubber molecules, leading to a reduction in the internal friction between the filler and rubber molecules and lowering the rolling resistance of the composites.

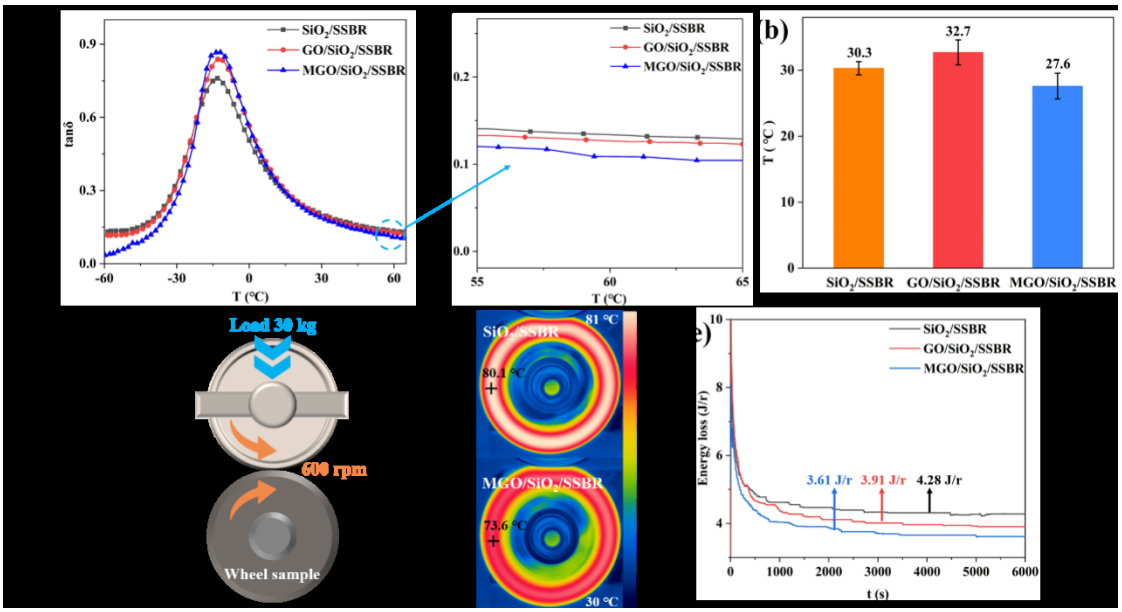

Figure 8. (a) Loss factor-temperature curves of SiO_2/SSBR, GO/SiO_2/SSBR and MGO/SiO_2/SSBR composites; (b) heat build-up of SiO_2/SSBR, GO/SiO_2/SSBR and MGO/SiO_2/SSBR composites;(c) a schematic of the rolling resistance tester; (d) infrared thermal images of wheels after rolling for 90 min; (e) energy loss of wheels constructed from SiO_2/SSBR, GO/SiO_2/SSBR and MGO/SiO_2/SSBR composites

Table 2. Loss factors of SiO_2/SSBR, GO/SiO_2/SSBR and MGO/SiO_2/SSBR composites

Temperature	SiO_2/SSBR	GO/SiO_2/SSBR	MGO/SiO_2/SSBR
0 °C	0.489	0.565	0.574
60 °C	0.134	0.127	0.108

The viscoelasticity of rubber composites also indicates their rolling resistance [31]. Specifically, tan δ values at 0 °C and 60 °C were used to predict the wet skid resistance and rolling resistance, respectively [32, 33]. Therefore, DMA was employed to determine the dynamic mechanical properties of rubber composites. Figure 8a and Table 1 show that

the tan δ values at 0 °C of the MGO/SiO_2/SSBR composite were increased by 17.3%, while the tan δ values at 60 °C decreased by 19.4%, compared with those of the SiO_2/SSBR composite. These results indicate that the wet skid resistance and rolling resistance of the MGO/SiO_2/SSBR composite improved, and this improvement was attributed to three factors. (1) The GO sheets promoted the dispersion of SiO_2, thereby reducing the mutual friction between the fillers. (2) The interfacial interaction between GO and rubber molecules was enhanced, thereby reducing the mutual friction between the filler and molecular chains. (3) The crosslinking density of the MGO/SiO_2/SSBR composite increased, thereby reducing the entanglement and mutual friction between the rubber chains.

Furthermore, to confirm the practical application of the MGO/SiO_2/SSBR composite as a tread material, the heat build-up and energy loss of the composites were investigated. Figure 8b shows that the heat build-up temperature of the GO/SiO_2/SSBR composite increased by 2.4 °C compared with that of the SiO_2/SSBR composite, suggesting that there is significant mutual friction between GO sheets and SiO_2 particles. However, the heat build-up temperature of the MGO/SiO_2/SSBR composite decreased by 5.1 °C compared with that of the GO/SiO_2/SBR composite, indicating that the strong interfacial interaction of fillers and rubber contributed to the reduction in friction between all components. Figure 8c provides a schematic of the rolling resistance tester. A load of 30 kg was applied to the wheel at a rotational velocity of 600 rpm. The infrared thermal images in Figure 8d show that the internal temperature (73.6 °C) of the MGO/SiO_2/SSBR wheel was lower than that of the SiO_2/SSBR wheel (80.1 °C). Accordingly, the corresponding energy loss of the MGO/SiO_2/SSBR wheel was measured at 3.61 J/r, indicating the energy saving was improved by 15.7% compared with the SiO_2/SSBR wheel. These results indicate that the chemical interface interaction between MGO and rubber molecules hinders the internal mutual friction in rubber composites [34-36], leading to low rolling resistance and heat build-up in the MGO/SiO_2/SSBR composite. Figure 9 depicts the mechanism diagram of the internal mutual friction in the SiO_2/SSBR and MGO/SiO_2/SSBR tire composites when a vehicle is driven.

A measure of the energy-saving efficiency of the tread rubber composites was obtained from the DMA and rolling resistance tester. The quantitative relationship between the energy loss (H) and $tan\delta$ of the tread rubber composites is given by Eq. 1 [37]:

$$H = \int_0^{2\pi/\omega} \sigma(t) \frac{d\varepsilon(t)}{dt} = \pi\sigma_\alpha \varepsilon_\alpha sin\delta \approx \pi\sigma_\alpha \varepsilon_\alpha tan\delta \quad (1)$$

where ω is the angular frequency; σ_α is the stress amplitude; ε_α is the strain amplitude; t is the time; δ is the phase difference between the strain and stress; and $tan\delta$ is the loss factor. The energy loss of the MGO/SiO_2/SSBR composite was calculated to be 3.38 J/r, which was lower than the calculated 4.39 J/r for the SiO_2/SSBR composite.

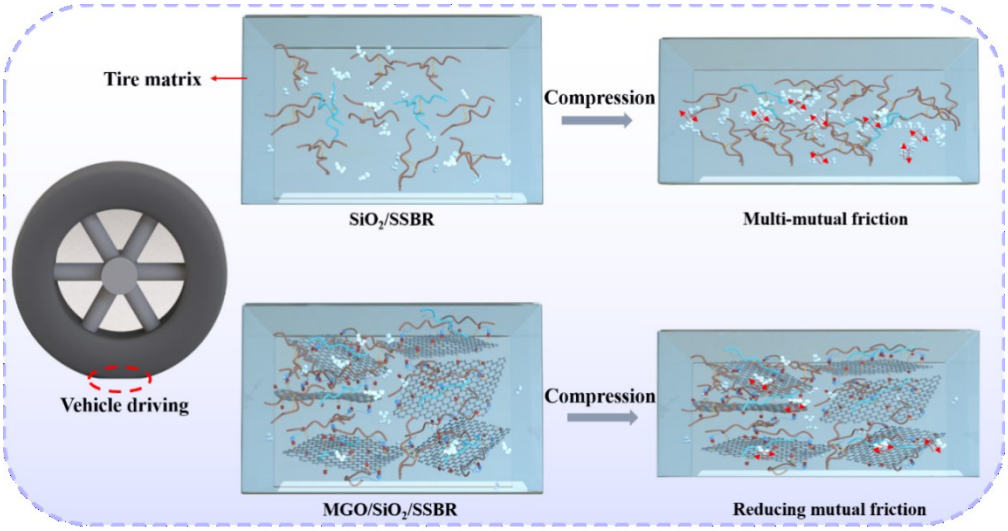

Figure 9. Internal mutual friction mechanism schematic of the SiO_2/SSBR and MGO/SiO_2/SSBR tire composites when a vehicle is driven

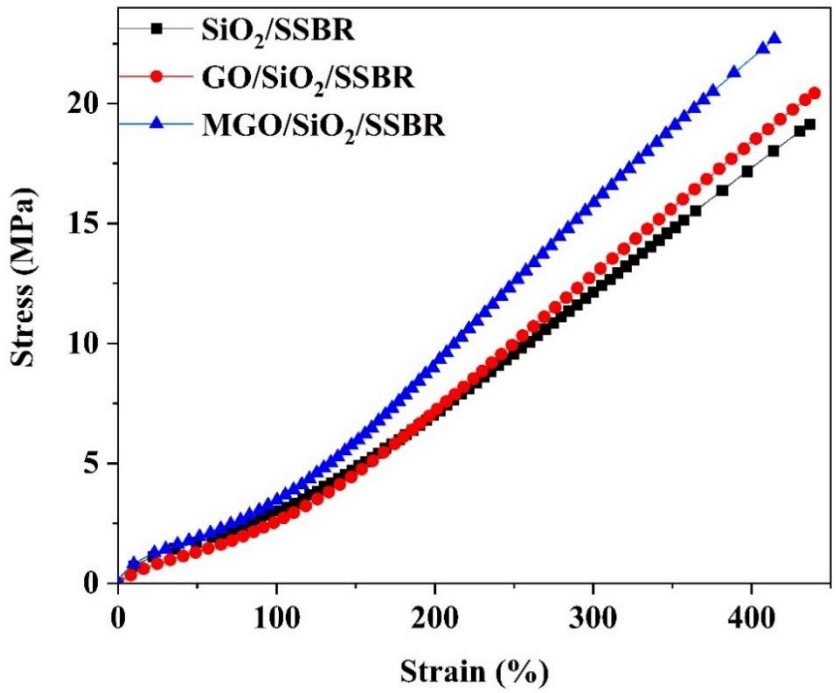

Figure 10. Stress-strain curves of different SSBR composites

Table 3. Mechanical property parameters of different SSBR composites

Samples	Shore A hardness	100% Modulus （MPa）	300% Modulus （MPa）	Tensile strength （MPa）	Elongation at break （MPa）	Tear strength （kN/m）
SiO_2/SSBR	59±1	2.9±0.2	12.1±0.1	19.1±0.3	436±18	38.1±1
GO/SiO_2/SSBR	63±1	2.6±0.3	12.9±0.1	20.4±0.2	440±22	39.3±1
MGO/SiO_2/SSBR	66±1	3.5±0.2	15.9±0.2	22.7±0.3	414±19	41.2±1

Figure 10 and Table 2 show the static mechanical properties of different SSBR composites. Compared to the SiO_2/SSBR composite, the 300% modulus and tensile strength of the MGO/SiO_2/SSBR composite increased by 31.4% and 18.8%, respectively. This was attributed to the strong chemical interface between MGO and rubber molecules. However, the elongation at break of the MGO/SiO_2/SSBR composite decreased, indicating that the rubber molecules were constrained to slip and reorient because of the strong chemical interfaces. In addition, the tear strength of the MGO/SiO_2/SSBR composite was higher than those of the other two composites, attributable to the introduction of MGO with large aspect ratios and strong interface interactions, which efficiently hindered the propagation of microcracks.

3.7 Abrasion performance of MGO/SiO_2/SSBR composites

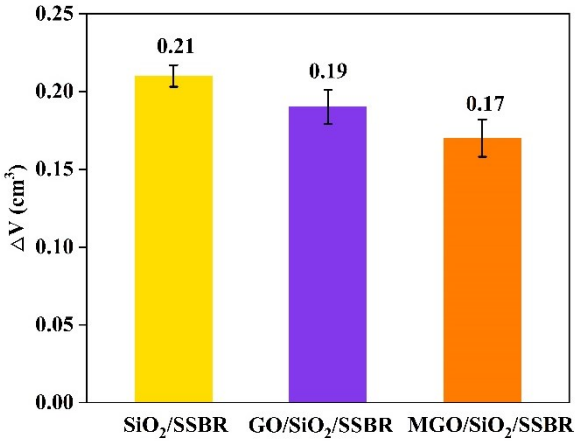

Figure 11. Abrasion performance of SiO_2/SSBR, GO/SiO_2/SSBR, and MGO/SiO_2/SSBR composites

Figure 11 shows the abrasion resistance of the SiO_2/SSBR, GO/SiO_2/SSBR, and MGO/SiO_2/SSBR composites. The wear performance of the MGO/SiO_2/SSBR composite is 19% higher than that for the SiO_2/SSBR composite. This was probably due to the MGO sheets contributing to the network crosslinking points, resulting in a high crosslinking density in the MGO/SiO_2/SSBR composite. Therefore, the slip and migration of rubber molecular chains were restricted, and the strength of the MGO/SiO_2/SSBR composite was enhanced, leading to an improvement in the abrasion resistance of the MGO/SiO_2/SSBR composites.

4. Conclusions

In this study, functionalized GO was evenly dispersed in SSBR composites, which promoted the dispersion of SiO_2 in rubber matrices, thereby reducing the mutual friction between silica and silica. The strong chemical interface between GO and the rubber molecules was formed by the thiol-vinyl click reaction at high temperatures. The MGO sheets also acted as crosslinking points and enhanced the crosslinking of the network. The fine filler dispersion and chemical interfaces reduce the mutual friction in the composites, further improving the rolling resistance and energy-saving properties of the rubber composite. The results showed that the rolling resistance of the MGO/SiO_2/SSBR composite increased by 19.4% relative to that of the SiO_2/SSBR composite. The wet skid

and abrasion resistances of the MGO/SiO_2/SSBR composite increased by 17.3% and 19%, respectively, relative to the SiO_2/SSBR composite. Overall, these results provide a feasible strategy for balancing the "magic triangle" properties and manufacturing green tires with energy-saving properties.

Acknowledgments

This work was supported by the National Key R&D Program of China (2017YFE0126800) and the National Natural Science Foundation of China (51790504).

References

[1] J. Jung, H.A. Sodano, Aramid Nanofiber Reinforced Rubber Compounds for the Application of Tire Tread with High Abrasion Resistance and Fuel Saving Efficiency, ACS Applied Polymer Materials 2(11) (2020) 4874-4884.

[2] J. Liu, Y.-L. Lu, M. Tian, F. Li, J. Shen, Y. Gao, L. Zhang, The Interesting Influence of Nanosprings on the Viscoelasticity of Elastomeric Polymer Materials: Simulation and Experiment, Advanced Functional Materials 23(9) (2013) 1156-1163.

[3] X. Qin, B. Han, J. Lu, Z. Wang, Z. Sun, D. Wang, T.P. Russell, L. Zhang, J. Liu, Rational design of advanced elastomer nanocomposites towards extremely energy-saving tires based on macromolecular assembly strategy, Nano Energy 48 (2018) 180-188.

[4] X. Zhai, Y. Chen, D. Han, J. Zheng, X. Wu, Z. Wang, X. Li, X. Ye, L. Zhang, New designed coupling agents for silica used in green tires with low VOCs and low rolling resistance, Applied Surface Science 558 (2021) 149819.

[5] X. Qin, J. Wang, Y. Zhang, Z. Wang, S. Li, S. Zhao, T. Tan, J. Liu, L. Zhang, K. Matyjaszewski, Self-Assembly Strategy for Double Network Elastomer Nanocomposites with Ultralow Energy Consumption and Ultrahigh Wear Resistance, Advanced Functional Materials 30(34) (2020).

[6] Official Journal of the European Union, L342 (2009) 46−58.

[7] Z. Tang, J. Huang, X. Wu, B. Guo, L. Zhang, F. Liu, Interface Engineering toward Promoting Silanization by Ionic Liquid for High-Performance Rubber/Silica Composites,

Industrial & Engineering Chemistry Research 54(43) (2015) 10747-10756.
[8] S. Fang, F. Li, J. Liu, L. Zhang, D. Wang, B. Liu, S. Wu, Z. Tang, B. Guo, Rubber-reinforced rubbers toward the combination of high reinforcement and low energy loss, Nano Energy 83 (2021).
[9] J. Zheng, D. Han, S. Zhao, X. Ye, Y. Wang, Y. Wu, D. Dong, J. Liu, X. Wu, L. Zhang, Constructing a Multiple Covalent Interface and Isolating a Dispersed Structure in Silica/Rubber Nanocomposites with Excellent Dynamic Performance, ACS Appl Mater Interfaces 10(23) (2018) 19922-19931.
[10] A.A. Hassan, K. Formela, S. Wang, Enhanced interfacial and mechanical performance of styrene-butadiene rubber/silica composites compatibilized by soybean oil derived silanized plasticization, Composites Science and Technology 197 (2020).
[11] Y. Shui, L. Huang, C. Wei, G. Sun, J. Chen, A. Lu, L. Sun, D. Liu, How the silica determines properties of filled silicone rubber by the formation of filler networking and bound rubber, Composites Science and Technology 215 (2021) 109024.
[12] B. Yoon, J.Y. Kim, U. Hong, M.K. Oh, M. Kim, S.B. Han, J.-D. Nam, J. Suhr, Dynamic viscoelasticity of silica-filled styrene-butadiene rubber/polybutadiene rubber (SBR/BR) elastomer composites, Composites Part B: Engineering 187 (2020) 107865.
[13] Y.C. Yong Lin, Zhikai Zeng, Jiarong Zhu, Yong Wei, Fucheng Li, Lan Liu, Effect of ZnO nanoparticles doped graphene on static and dynamic mechanical properties of natural rubber composites, Composites: Part A 70(24) (2015) 35-44.
[14] B. Zhong, Y. Luo, W. Chen, Y. Luo, D. Hu, H. Dong, Z. Jia, D. Jia, Immobilization of rubber additive on graphene for high-performance rubber composites, J Colloid Interface Sci 550 (2019) 190-198.
[15] P. Liu, X. Zhang, H. Jia, Q. Yin, J. Wang, B. Yin, Z. Xu, High mechanical properties, thermal conductivity and solvent resistance in graphene oxide/styrene-butadiene rubber nanocomposites by engineering carboxylated acrylonitrile-butadiene rubber, Composites Part B: Engineering 130 (2017) 257-266.
[16] Z. Xu, L. Zheng, S. Wen, L. Liu, Graphene oxide-supported zinc oxide nanoparticles for chloroprene rubber with improved crosslinking network and mechanical properties, Composites Part A: Applied Science and Manufacturing 124 (2019).

[17] G. Yang, Z. Liao, Z. Yang, Z. Tang, B. Guo, Effects of substitution for carbon black with graphene oxide or graphene on the morphology and performance of natural rubber/carbon black composites, Journal of Applied Polymer Science 132(15) (2015).

[18] H. Zhang, Y. Wei, Z. Kang, G. Zhao, Y. Liu, Influence of partial substitution for carbon black with graphene oxide on dynamic properties of natural rubber composites, Micro & Nano Letters 12(9) (2017) 605-610.

[19] Y. Zou, J. He, Z. Tang, L. Zhu, F. Liu, Structural and mechanical properties of styrene–butadiene rubber/silica composites with an interface modified in-situ using a novel hindered phenol antioxidant and its samarium complex, Composites Science and Technology 188 (2020).

[20] H. Guo, S. Jerrams, Z. Xu, Y. Zhou, L. Jiang, L. Zhang, L. Liu, S. Wen, Enhanced fatigue and durability of carbon black/natural rubber composites reinforced with graphene oxide and carbon nanotubes, Engineering Fracture Mechanics 223 (2020).

[21] H. Wang, H. Zhang, J. Zhang, Y. Zhao, Improving tribological performance of fluoroether rubber composites by ionic liquid modified graphene, Composites Science and Technology 170 (2019) 109-115.

[22] L. Chu, M. Kan, S. Jerrams, R. Zhang, Z. Xu, L. Liu, S. Wen, L. Zhang, Constructing Chemical Interface Layers by Using Ionic Liquid in Graphene Oxide/Rubber Composites to Achieve High-Wear Resistance in Environmental-Friendly Green Tires, ACS Appl Mater Interfaces 14(4) (2022) 5995-6004.

[23] L. Zheng, S. Jerrams, T. Su, Z. Xu, L. Zhang, L. Liu, S. Wen, Enhanced covalent interface, crosslinked network and gas barrier property of functionalized graphene oxide/styrene-butadiene rubber composites triggered by thiol-ene click reaction, Composites Part B: Engineering 197(13) (2020) 186-195.

[24] Z. Xu, S. Jerrams, L. Zheng, L. Zhang, L. Liu, S. Wen, Green Fabrication of High-Performance, Lignosulfonate-Functionalized, and Reduced-Graphene Oxide Styrene–Butadiene Rubber Composites, Industrial & Engineering Chemistry Research 60(49) (2021) 17989-17998.

[25] Y. Wang, W. Wang, R. Xu, M. Zhu, D. Yu, Flexible, durable and thermal conducting thiol-modified rGO-WPU/cotton fabric for robust electromagnetic interference shielding,

Chemical Engineering Journal 360 (2019) 817-828.
[26] Q. Li, G. Lin, S. Chen, L. Zhang, Y. Song, C. Geng, S. Qu, Y. Jing, F. Liu, Z. Liang, Enhancing mechanical performance and wet-skid resistance of emulsion styrene butadiene rubber/natural rubber latex composites via in-situ hybridization of silanized graphene oxide and silica, Journal of Applied Polymer Science 139(18) (2022).
[27] X. Shang, Y. Zhu, Z. Li, Surface modification of silicon carbide with silane coupling agent and hexadecyl iodiele, Applied Surface Science 394 (2017) 169-177.
[28] R. Bellas, J. Díez, M. Rico, L. Barral, C. Ramírez, B. Montero, Accelerated ageing of styrene-butadiene rubber nanocomposites stabilized by phenolic antioxidant, Polymer Composites 35(2) (2014) 334-343.
[29] C. Zhang, Z. Tang, B. Guo, L. Zhang, Significantly improved rubber-silica interface via subtly controlling surface chemistry of silica, Composites Science and Technology 156 (2018) 70-77.
[30] L. Zheng, S. Jerrams, Z. Xu, L. Zhang, L. Liu, S. Wen, Enhanced gas barrier properties of graphene oxide/rubber composites with strong interfaces constructed by graphene oxide and sulfur, Chemical Engineering Journal 383 (2020) 123100.
[31] S. Bhadra, S. Nair, Tailor-made one-part epoxy resin for tire compound to improve ride and handling and reduce rolling resistance, Materials Today: Proceedings 62 (2022) 7002-7006.
[32] L. Wang, S. Zhao, A. Li, X. Zhang, Study on the structure and properties of SSBR with large-volume functional groups at the end of chains, Polymer 51(9) (2010) 2084-2090.
[33] S.Z. Xiao Liu , Xingying Zhang , Xiaolin Li , Yu Bai Preparation, structure, and properties of solution-polymerized styrene-butadiene rubber with functionalized end-groups and its silica-filled composites, Polymer 55(4) (2014) 1964-1976.
[34] P. Weng, Z. Tang, B. Guo, Solving “magic triangle” of tread rubber composites with phosphonium-modified petroleum resin, Polymer 190 (2020).
[35] A. Samadi, M. Razzaghi Kashani, M.H.N. Famili, Design, construction, and evaluation of a modified rolling pendulum to measure energy dissipation in rubber, Polymer Testing 35 (2014) 56-61.

[36] X. Qin, H. Xu, G. Zhang, J. Wang, Z. Wang, Y. Zhao, Z. Wang, T. Tan, M.R. Bockstaller, L. Zhang, K. Matyjaszewski, Enhancing the Performance of Rubber with Nano ZnO as Activators, ACS Appl Mater Interfaces 12(42) (2020) 48007-48015.

[37] W. Lei, X. Zhou, T.P. Russell, K.-c. Hua, X. Yang, H. Qiao, W. Wang, F. Li, R. Wang, L. Zhang, High performance bio-based elastomers: energy efficient and sustainable materials for tires, Journal of Materials Chemistry A 4(34) (2016) 13058-13062.